Emerin Dysregulation Drives the Very-Small-Nuclear Phenotype and Lineage Plasticity That Associate with a Clinically Aggressive Subtype of Prostate Cancer

Le Zhang[1,2], Pai-Chi Teng[3], Karen A. Cavassani[1,2], Jasmine Wang[1,2], Catherine Grasso[1,2], Joshua Watson[1,2], Zijing Chen[1,2], Kai-Han Tu[1,2], Brenda Salumbides[1,2], Krizia Rohena-Rivera[1,2], Lilit Gevorkian[1,2], Minhyung Kim[1,4], Sungyong You[1,4], Dolores Di Vizio[1,4,5], Howard M. Sandler[1,6], Timothy Daskivich[1,4], Neil A. Bhowmick[1,2,4], Michael R. Freeman[1,4,5], Hsian-Rong Tseng[7], Jie-Fu Chen[8], and Edwin M. Posadas[1,2,4,9]

ABSTRACT

Purpose: Circulating tumor cells (CTC) with a very-small-nuclear phenotype (vsnCTC) in prostate cancer are characterized by nuclei smaller than 8.5 μm. Our previous studies established an association between vsnCTCs and visceral metastasis. Reduction of emerin (EMD), a nuclear envelope protein, contributes to prostate cancer metastasis and nuclear shape instability. In this study, we investigated the correlation between EMD expression and the vsnCTC phenotype and its clinical impact.

Experimental Design: We analyzed CTCs from 93 patients with metastatic castration-resistant prostate cancer and categorized them as either vsnCTC+ or vsnCTC− and compared overall survival and progression-free survival. C4-2B, 22Rv1, and DU145 with EMD knockdown were developed and characterized by nuclear size and gene expression by gene set enrichment analysis. Abiraterone- and enzalutamide-resistant C4-2B cells were also characterized by nuclear size and EMD expression.

Results: Patients who were vsnCTC+ had significantly worse overall survival and progression-free survival compared with patients who were vsnCTC−. EMD expression was markedly reduced in CTCs from patients who were vsnCTC+ compared with patients who were vsnCTC−, with a significant positive correlation between EMD expression and CTC nuclear size. EMD knockdown in prostate cancer cells resulted in smaller nuclei, enhanced invasion, and the upregulation of genes associated with lineage plasticity. Additionally, abiraterone- and enzalutamide-resistant C4-2B cells had smaller nuclei and lower EMD expression. vsnCTC+ cells also showed enhanced platinum sensitivity.

Conclusions: The presence of vsnCTCs represents a novel hallmark of an aggressive subtype of metastatic castration-resistant prostate cancer closely linked to EMD loss and lineage plasticity. These findings highlight the importance of EMD dysregulation in the vsn phenotype, disease progression, and therapeutic resistance in patients with prostate cancer.

[1]Center for Uro-Oncology Research Excellence, Cedars-Sinai Cancer, Los Angeles, California. [2]Division of Medical Oncology, Department of Medicine, Cedars-Sinai Medical Center, Los Angeles, California. [3]Division of Urology, Department of Surgery, Cardinal Tien Hospital, Fu Jen Catholic University, Taipei, Taiwan. [4]Department of Urology, Cedars-Sinai Medical Center, Los Angeles, California. [5]Department of Biomedical Sciences, Cedars-Sinai Medical Center, Los Angeles, California. [6]Department of Radiation Oncology, Cedars-Sinai Medical Center, Los Angeles, California. [7]Department of Molecular and Medical Pharmacology, California NanoSystems Institute, Crump Institute for Molecular Imaging, University of California, Los Angeles, Los Angeles, California. [8]Department of Pathology, Memorial-Sloan Kettering Cancer Center, New York, Ney York. [9]Cancer Therapeutics Program, Cedars-Sinai Cancer, Los Angeles, California.

L. Zhang, P.-C. Teng, and K.A. Cavassani contributed equally to this article.

J.-F. Chen and E.M. Posadas contributed equally to this article.

Corresponding Author: Edwin M. Posadas, Cancer Therapeutics Program & Center for Uro-Oncology Research Excellence, Cedars-Sinai Cancer, Division of Medical Oncology, Department of Medicine & Department of Urology, Cedars-Sinai Medical Center, 8700 Beverly Boulevard, Los Angeles, CA 90048. E-mail: Edwin.Posadas@csmc.edu

Clin Cancer Res 2025;31:2034–45

doi: 10.1158/1078-0432.CCR-24-3660

Introduction

Circulating tumor cells (CTC) are cells that shed from the primary tumor and enter the bloodstream, playing a critical role in the process of metastasis (1, 2). Detecting CTCs from clinical samples through liquid biopsy provides a valuable tool for cancer diagnosis and prognosis. In prostate cancer, a key limitation of using serum PSA as a biomarker is its dependence on androgen levels (3). In contrast, CTCs are not influenced by androgen receptor (AR)–mediated signaling, making them a more reliable marker for monitoring tumor spread (4). Our team used a nanotechnology-enabled analysis to identify a unique population of CTCs in prostate cancer, characterized by very small nuclei (less than 8.5 μm in size), known as vsnCTCs (5–7). These vsnCTCs were found to emerge during disease progression under intensive AR suppression with AR signaling inhibitors (ARSI) and were linked to the presence of visceral metastases (VM), including spread to the liver, lungs, or other soft tissue sites, in advanced metastatic castration-resistant prostate cancer (mCRPC; ref. 5). VM are associated with poor clinical outcomes and frequently observed in patients with treatment-emergent neuroendocrine prostate cancer (8, 9).

Lineage plasticity, the ability of cancer cells to transition from one differentiated cell type to another, is a key mechanism of cancer adaptation (10). In prostate cancer, this plasticity often leads to resistance to treatments like androgen deprivation therapy, resulting

Translational Relevance

This study extends the clinical and biological insights into the very-small-nuclear phenotype circulating tumor cell (vsnCTC), a CTC biomarker denoted by its distinctly small nuclear size. The presence of the vsnCTCs is associated with poor clinical outcomes and has loss/dysregulation of emerin as a biological feature. Dysregulation of emerin and the presence of a vsn phenotype in CTCs may provide new insights into emerging tumor plasticity and progression. Characterization of this biology in the circulation may aid in refining risk stratification and guiding treatment selection, particularly identifying patients who are more likely to benefit from platinum-based chemotherapy. These findings underscore the potential of characterizing CTCs to advance precision oncology and justify further studies to explore its utility in personalizing prostate cancer therapy.

in the emergence of cellular phenotypes with decreased dependence on AR–ligand stimulation, such as neuroendocrine or small cell carcinoma (11). In this study, we continued our previous study to investigate the presence of lineage plasticity markers in the vsnCTC phenotype cells.

Morphologic changes, including alterations in nuclear size, have been linked to invasive and aggressive prostate cancer (12–14). These changes result from variations in the composition of the nuclear matrix and envelope. Previous studies have shown that nuclear alterations can predict metastasis and mortality in patients with prostate cancer (13, 15, 16), which aligns with our own findings. It has also been reported that metastatic cancer cells exhibit both structural and compositional changes in nuclear envelope proteins (17). Emerin (EMD), a key component of the nuclear envelope, plays a significant role in maintaining nuclear integrity (18, 19). Our group previously identified low expression of EMD in CTCs from metastatic patients with prostate cancer, with EMD deficiency being associated with more aggressive disease (20). This deficiency of EMD in prostate cancer cells was linked to nuclear shape instability and an amoeboid phenotype that enhances metastatic potential (20). Based on these observations, we hypothesize that EMD loss contributes to the vsn phenotype in CTCs and prostate cancer cell lines, characterized by reduced nuclear size, increased invasiveness, and lineage plasticity. This, in turn, leads to increased metastatic capacity and poorer clinical outcomes. Understanding the biological mechanisms behind this phenotype may serve as a valuable prognostic tool, enabling the timely implementation of effective therapies and improving patient outcomes.

Materials and Methods

Patient selection and study design

Human investigations were performed after approval by the Cedars-Sinai Medical Center Institutional Review Board. All patients provided written informed consent prior to any research collection. Under Institutional Review Board# Pro00042197, blood samples from consenting patients with mCRPC were collected for CTC analysis. This study was conducted in accordance with the Declaration of Helsinki and Good Clinical Practice guidelines. For this analysis, samples were considered usable if the following criteria were met: (i) a verified diagnosis of prostate cancer with metastasis, (ii) disease progression with serum testosterone concentration <50 ng/dL (i.e., castration), and (iii) clinical follow-up data on progression/death available. Samples were only collected from patients receiving care at the Cedars-Sinai Cancer Center for Uro-Oncology Research Excellence clinics to ensure access to clinical outcome data. Samples collected between September 2014 and June 2018 were considered for inclusion. Samples were included in the overall survival (OS) analysis if CTC assessment by NanoVelcro assay was performed and confirmed by an experienced, clinical pathologist. Moreover, the CTCs need to be suitable for characterization as vsnCTC positive (+) or negative (−). A subgroup of samples was utilized for an analysis of disease progression while on treatment (i.e., progression-free survival, PFS) if the patient started treatment within 4 weeks of blood collection. All treatments and examinations (laboratory and radiographic) were performed as part of standard care. Only one sample was collected per patient for all analyses in this study. The demographics and clinical characteristics of these patients at the time of blood draw have been summarized in **Table 1**.

CTC enrichment, imaging, and nuclear size measurements

The workflow and detailed methods for CTC enrichment and vsnCTC enumeration have been summarized in Supplementary Fig. S1. In short, venous blood of patients was collected in acid-citrate-dextrose–containing vacutainers and processed within 24 hours of phlebotomy. Following density gradient centrifugation using a Ficoll-Paque solution (Sigma-Aldrich) per the manufacturer's specifications, the peripheral blood mononuclear cell layer was isolated. The peripheral blood mononuclear cells (up to 2 mL of whole blood equivalent) were then loaded into a NanoVelcro CTC assay chip to enrich CTCs using our previously published protocol (6). The captured cells were then fixed with 2% paraformaldehyde and subjected to immunocytochemical staining. Candidate CTCs were characterized as 4′,6-diamidino-2-phenylindole (DAPI)–positive/cytokeratin (CK)-positive/CD45-negative cells with round or oval nuclei using an upright fluorescence microscope (Eclipse 90i, Nikon Instruments Inc.). As apoptotic CTCs have been shown to be associated with patient outcomes in cancer (21, 22), each candidate was reviewed and certified by an experienced pathologist for morphology to specifically confirm that the observed event was a CTC (rather than a hematologic cell) and lacked features of apoptosis. Nuclear size was defined as the square root of the product of the long axis and the short axis. The calibration studies for ensuring the accuracy and reproducibility of nuclear size measurements on NanoVelcro CTC assay were conducted in our previous study using prostate cancer cell lines and patient samples (6). A vsnCTC was defined as a CTC with nuclear size less than 8.5 μm based on our previous work (5). In this study, we explored the relationship of OS to minimum, median, and mean CTC nuclear size, as defined by the smallest, median, and average nuclear size among the CTCs obtained in each enumeration study/blood specimen, respectively.

Cell lines

C4-2B cells resistant to enzalutamide (Enza-R) or abiraterone (Abi-R) as well as control (parental) cells were kindly provided by Dr. Allen Gao (University of California Davis, CA). C4-2B/Enza-R cells were maintained in 20 μmol/L Enza-containing medium as previously described (23). C4-2B/Abi-R cells were maintained in 10 μmol/L Abi. C4-2B (RRID: CVCL_4784), DU145 (RRID: CVCL_0105), and 22Rv1 (RRID: CVCL_1045) cells were purchased from ATCC. C4-2B and 22Rv1 were maintained in RPMI-1640 medium with 10% FBS and 1% penicillin/streptomycin. DU145 were cultured in DMEM (Thermo Fisher Scientific) with 10% FBS and 1% penicillin/streptomycin. EMD knockdown DU145 cells, generated by short hairpin RNA (shRNA),

Table 1. Patient characteristics (parentheses indicate the age range or percentage of the patients represented for each column).

Characteristic	Total (*N* = 93)	vsnCTC+ (*N* = 56)	vsnCTC− (*N* = 37)	*P* value
Age, median (range), years	73 (49–92)	73 (50–92)	73 (49–85)	NA
Race (%)				
White	73 (78)	44 (79)	29 (78)	
Black/African American	12 (13)	9 (16)	3 (8)	
Asian	5 (5)	1 (2)	4 (11)	0.2656
American Indian or Alaska Native	2 (2)	1 (2)	1 (3)	
Unknown	1 (1)	1 (2)	0 (0)	
Sites of disease (%)				0.0192
Bone ± lymph node only	48 (52)	23 (41)	25 (68)	
Any VM[a]	45 (48)	33 (59)	12 (32)	
Liver metastases	14 (15)	10 (18)	4 (11)	
Liver metastases only	9 (10)	8 (14)	1 (3)	
Lung metastases only	6 (6)	3 (5)	3 (8)	
VM only	16 (17)	11 (20)	5 (14)	
Prior treatment (%)				
ARSI(s)	61 (66)	41 (73)	20 (54)	
Abi	45 (48)	30 (54)	15 (41)	
Enza	35 (38)	24 (43)	11 (30)	
Apalutamide	8 (9)	8 (14)	0 (0)	0.4154
Darolutamide	1 (1)	1 (2)	0 (0)	
Taxane	33 (35)	24 (43)	9 (24)	
Docetaxel	32 (34)	24 (43)	8 (22)	
Cabazitaxel	12 (13)	9 (16)	3 (8)	
Radium-223	15 (16)	8 (14)	7 (19)	
Treatment to be received after vsnCTC assessment or current treatment (%)[b]				0.2985
ARSI(s)	52 (56)	28 (50)	24 (65)	
Abi	26 (28)	15 (27)	11 (30)	
Enza	19 (20)	8 (14)	11 (30)	
Apalutamide	7 (8)	5 (9)	2 (5)	
Taxane	22 (24)	16 (29)	6 (16)	
Docetaxel	15 (16)	12 (21)	3 (8)	
Cabazitaxel	7 (8)	4 (7)	3 (8)	
Platinum	4 (4)	2 (4)	2 (5)	
Lines of CRPC treatments prior to vsnCTC assessment (%)				
0 or 1 line	42 (45)	20 (36)	22 (59)	0.0334
2+ lines	51 (55)	36 (64)	15 (41)	

[a]Metastasis to any visceral site with or without bone and/or lymph node metastases.
[b]For all the subsequent treatment, please see Supplementary Table S3.

were kindly provided by Dr. Michael R. Freeman (20). All cultures were grown in a humidified 5% CO_2 environment at 37°C. Cell line authentication was conducted by ATCC and periodically tested using the *Mycoplasma* Detection Kit (Lonza), and cells were clear of contamination.

siRNA transfection

C4-2B, 22Rv1, and DU145 cells were transfected with *EMD* siRNA (sc-35296, Santa Cruz Biotechnology; RRID: SCR_026442) and control scramble siRNA (sc-37007, Santa Cruz; RRID: SCR_026443) using Lipofectamine 3000 (Thermo Fisher Scientific), as described by the manufacturer. Then, 24 hours after the addition of the transfection mix, liposomes were removed, and fresh medium was added.

Immunofluorescence

Cells were seeded on poly-L-lysin (Sigma-Aldrich) coated Nunc Lab-Tek plates (Thermo Fisher Scientific), then fixed with 2% paraformaldehyde and subjected to immunocytochemical staining as previously described (20). Images were captured using a Leica DMi8 fluorescence microscope and ImageJ (RRID: SCR_003070) was used to measure nuclear size.

Transwell invasion assays

Cells were fasted in 0.1% BSA and then plated (0.1×10^6) on transwell inserts (8 μm) coated with Matrigel matrix, phenol red free (BD Biosciences). Inserts were then placed in 24-well plates containing 5% FBS and incubated at 37°C for 24 to 48 hours. After incubation, media were aspirated, and cells which did not invade through the chamber on the upper side of the membrane were removed with a swab. Cells attached to the bottom side of the membrane were fixed with 4% paraformaldehyde and stained with 0.1% (v/v) crystal violet. Inserts were washed and photographed at 10× using an inverted microscope (Leica) and MagnaFire SP software. Transwell assays were performed independently at least 3 times.

RNA preparation, cDNA synthesis, and qPCR

Cell lines were lysed in TRIzol (Life Technologies, Invitrogen), and total RNA was prepared using Direct-zol RNA MicroPrep

(Zymo Research) according to manufacturer's instructions. 500 ng of total RNA was reverse-transcribed, and cDNA was used for qPCR analysis on a QuantStudio 5 Real-Time PCR system (Applied Biosystems; RRID: SCR_021096) per the manufacturer's instructions. In all cases, target gene expression was normalized to the expression of housekeeping genes such as *GAPDH*. Relative gene expression was calculated using standard $2-\delta\delta Ct$. Results were generated from at least three independent experiments and are shown as the mean ± SD. Primers used are listed in Supplementary Table S1.

RNA sequencing and gene set enrichment analysis

Total RNA was extracted with the RNeasy Plus Mini Kit (Qiagen; RRID: SCR_008539) according to the manufacturer's instructions. All the RNA sequencing (RNA-seq) experiments were performed in triplicate. RNA library and transcriptome sequencing were performed by Novogene. Gene set enrichment analysis (GSEA; RRID: SCR_003199) of differentially expressed genes was performed by GSEA 4.0.3. Code and relevant data have been deposited in Code Ocean at: /https://codeocean.com/capsule/7045784/tree/v1.

MTT [3-(4,5-dimethylthiazol-2-yl)-2,5-diphenyltetrazolium bromide] assay

C4-2B cells were transfected with either siRNA targeting EMD or control siRNA. Following transfection, the cells were cultured in the presence of Abi acetate (10 μmol/L; 99%, MedKoo Biosciences) or Enza (1 μmol/L). Cell viability was assessed on day 5 of culture using the MTT assay, following the manufacturer's instructions (Thermo Fisher Scientific).

Lentivirus infection

Lentiviral shRNA transduction particles targeting human EMD and lentiviral nontargeting control transduction particles (SHC002V) were purchased from Sigma. The EMD shRNA was a pool of five different siRNA target sequences:

EMD shRNA #1 (oligo ID: TRCN0000083010) hairpin sequence: 5′-AAACCCAGGGCTGCCTTGGAAAAG-3′; EMD shRNA #2 (oligo ID: TRCN0000083011) hairpin sequence: 5′- AAACCCAGGGCTGCCTTGGAAAAG-3′; EMD shRNA #3 (oligo ID: TRCN0000083008) hairpin sequence: 5′-GTTGACATGCATTCCTCCTTT-3′; EMD shRNA #4 (oligo ID: TRCN0000083009) hairpin sequence: 5′-CCCAAGAAAGAGGACGCTTTA-3′; and EMD shRNA #5 (oligo ID: TRCN0000083012) hairpin sequence: 5′-AGGTGCATGATGACGATCTTT-3′. Prostate cancer cells transducted with lentiviruses were supplemented with 8 μg/mL polybrene and then selected by puromycin for 3 to 5 days.

Western blotting

Extracted proteins were separated by 4% to 20% SDS-PAGE gels. The blots were probed with antibodies against EMD (6080531, Leica; RRID: AB_3676183) and β-actin (47778, Santa Cruz Biotechnology; RRID: AB_626632), followed by incubation with alkaline phosphatase-conjugated secondary antibodies (A3687, Sigma-Aldrich; RRID: AB_258103), or HRP anti-mouse (7076, Cell Signaling Technology; RRID: AB_330924) for 1 hour at room temperature. Blots were developed with an ECL substrate (Thermo Fisher Scientific, A38554) and chemiluminescence or by 1-step NBT/BCIP (34042, Thermo Fisher Scientific).

Cisplatin sensitivity assay

To exclude the presence of necrotic or apoptotic cells, DU145 EMD knockdown and control cells by shRNA were stained using the APC Annexin V Apoptosis Detection Kit with PI (BioLegend) and immediately sorted by FACS based on their negative expression of Annexin V/PI. These sorted cells were then used for the cisplatin sensitivity assay.

A total of 1×10^4 DU145 EMD knockdown and control cells by shRNA were seeded in a 96-well plate 16 hours before the addition of Cytotox Green (250 nmol/L) and different concentrations of cisplatin (0, 2, 10, and 50 μmol/L). Dying cells are labeled green, in real time, by the mix-and-read Incucyte Cytotox Green Dye. Images were collected every 2 hours, and the analysis was performed using Incucyte Cell-by-Cell Analysis Software Module, thus enabling individual cell segmentation and classification based on fluorescence. The increase of cell death is directly related to the increase of fluorescence area calculated by Incucyte software analysis.

Statistical analyses

Patients were designated as vsnCTC present/vsnCTC+ or vsnCTC absent/vsnCTC−. If a patient had ≥1 vsnCTC, this patient would be designated as vsnCTC+ regardless of the quantity of vsnCTCs or the presence of non-vsnCTCs. The Kaplan–Meier plot and log-rank test were used for OS and PFS analyses. OS was defined as the time from blood draw to time of death. Progression was defined as clinical progression (per the treating physician) or biochemical/radiographic progression according to Prostate Cancer Working Group 3 (ref. 24) and the RECIST1.1 (ref. 25). Multivariable Cox regression was used primarily to investigate the association of vsnCTC status with time to death and progression. To minimize bias from confounding factors, a model adjusting for the vsnCTC status, age, PSA, lines of CRPC treatment prior to the blood draw, and presence of VM at the time of blood draw was chosen. The results were shown as an HR with 95% confidence intervals (CI). A p-spline plot (26) was used to depict the association between the HR of OS and the CTC nuclear size. Continuous variables were summarized as medians and IQRs and compared using the Mann–Whitney U test. A two-tailed Student *t* test was used for comparisons between two groups, whereas one-way ANOVA was used for comparisons among three or more groups. Results were presented as the mean ± SD, with $P < 0.05$ considered statistically significant. All data were analyzed from at least three independent experiments. Graphs were created using GraphPad Prism 9 software (RRID: SCR_002798).

Data availability

RNA-seq data are available at Gene Expression Omnibus with accession ID GSE288991. Additional data generated in this study are available upon request to the corresponding author.

Results

Patients with vsnCTCs have poor survival and exhibit increased resistance to AR-targeted therapy

Our initial study pointed to a relationship between the presence of vsnCTCs and VM (5). In this follow-up series, 93 clinically annotated, blood samples from patients with mCRPC with survival follow-up to death (if applicable) within the Translational Oncology Program Blood & Biospecimen Bank were selected for analysis. CTCs were isolated and analyzed using the NanoVelcro assay. Patient characteristics are shown in **Table 1**.

Among 93 patients, 77 (83%) had detectable CTCs, 56 (60%) were vsnCTC+, and 37 (40%) were vsnCTC−. 33 (59%) patients who were vsnCTC+ and 12 (32%) patients who were vsnCTC− had VM

at the time of blood draw ($P = 0.0192$). Interestingly, we also found that patients with mCRPC with greater than two lines of CRPC treatments prior to blood draw had greater vsnCTC positivity ($P = 0.0334$). Given the established relationship between VM and survival, we hypothesized that there was an association between vsnCTCs, OS, and PFS in mCRPC. As shown in **Fig. 1A**, vsnCTC+ had significantly shorter OS when compared with patients who were vsnCTC− (median 7.5 vs. 35.8 months, HR = 2.26, 95% CI, 1.46–3.50, log-rank $P = 0.0002$). After adjusting for potential confounding factors using a multivariate Cox regression model (i.e., PSA, presence of VM at blood draw, prior CRPC treatment line, age, and total CTC number per 1 mL of blood), vsnCTC+ status was independently associated with worse OS (Supplementary Table S2, HR = 1.70, 95% CI, 1.03–2.81, $P = 0.0396$). Treatments provided after vsnCTC assessment are provided in **Table 1** and Supplementary Table S3. In general, there were no patterns of treatment variation between the vsnCTC+ and vsnCTC− group over the natural history of their disease course. Patients with vsnCTC+ also had significantly shorter PFS compared with patients who were vsnCTC− (**Fig. 1B**, median 3.0 vs. 6.5 months, HR = 1.93, 95% CI, 1.13–3.28, log-rank $P = 0.0117$). To address potential overlap from our pervious vsnCTC study (5), we

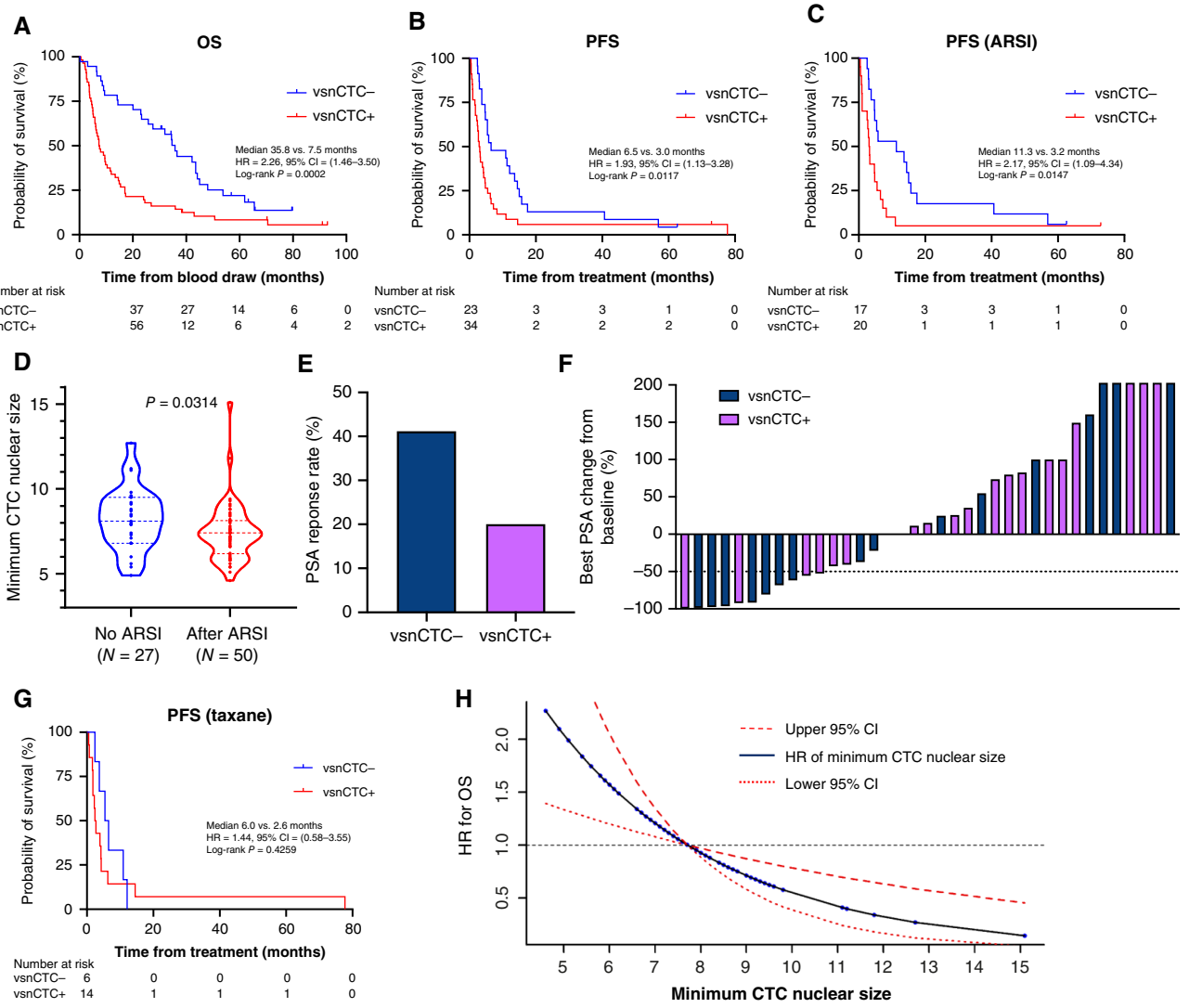

Figure 1.

vsnCTCs are associated with poorer clinical outcomes in advanced prostate cancer. Kaplan–Meier analysis of (**A**) OS for all patients with mCRPC ($N = 93$) with available blood specimens and (**B**) PFS for patients with available blood specimens prior to treatment of ARSIs or taxane therapy ($N = 57$). **C,** PFS for patients with available blood specimens prior to treatment of ARSIs ($N = 37$). **D,** Minimum CTC nuclear size of patients with and without prior ARSI therapy (median 7.4 vs. 8.1 μm). **E,** PSA response rate (%) in patients who were vsnCTC− (41%, $n = 17$) and vsnCTC+ (20%, $n = 20$). **F,** Best PSA change from baseline (prior ARSI therapy). Calculated from lowest PSA value at any time after baseline while on ARSI treatment by individual patients. The value was truncated at 200%. **G,** PFS for patients with available blood specimens prior to taxane therapy ($N = 20$). **H,** P-spline curve comparing minimum CTC nuclear size and HR for OS. As the minimum CTC nuclear size decreases, the HR (multivariate Cox proportional hazard model adjusting for age and PSA) of OS increases.

performed OS and PFS analyses excluding the 18 patients from the original study (Supplementary Fig. S2). Consistently, patients who were vsnCTC+ had significantly poorer OS and PFS. When specifically considering ARSI treatment, patients who were vsnCTC+ had significantly worse PFS compared with patients who were vsnCTC− (**Fig. 1C**, median 3.2 vs. 11.3 months, HR = 2.17, 95% CI, 1.09–4.34, log-rank $P = 0.0147$). Moreover, the CTC nuclear size was significantly smaller in patients with prior ARSI use compared with those with no prior ARSI use (median 7.4 vs. 8.1 μm, rank-sum test $P = 0.0314$, **Fig. 1D**). The patients with vsnCTC+ had a lower PSA response rate to ARSI treatment, compared with patients who were vsnCTC− (**Fig. 1E**). Accordingly, the best PSA change from baseline in each ARSI patient, as shown in the waterfall plot in **Fig. 1F**, revealed that among the 20 patients who were vsnCTC+, 2 (10%), 4 (20%), and 6 (30%) achieved a best PSA percentage decrease of 90% or more, 50% or more, and 30% or more, respectively. In contrast, of the 17 patients who were vsnCTC−, 4 (24%), 7 (41%), and 8 (47%) achieved a best PSA percentage decrease of 90% or more, 50% or more, and 30% or more, respectively.

In contrast to this, we considered the association between vsnCTC presence and taxane sensitivity. Here, there were fewer patients and in the available dataset, there was no statistically significant association between vsnCTC status and OS of patients receiving taxane therapy (**Fig. 1G**, median 2.5 vs. 6.0 months, HR = 1.44, 95% CI, 0.58–3.55, log-rank $P = 0.4259$). To test the hypothesis that a smaller minimum CTC nuclear size is associated with poorer prognosis, a p-spline plot was used to illustrate the relationship between OS and minimum CTC nuclear size (**Fig. 1H**). Generally, the HR of OS increased as the minimum CTC nuclear size decreased. Mean or median CTC nuclear size did not show a significant association with the HR for OS. Additionally, we performed a p-spline analysis to explore the relationship between CTC number and OS. The p-spline analysis revealed a trend toward

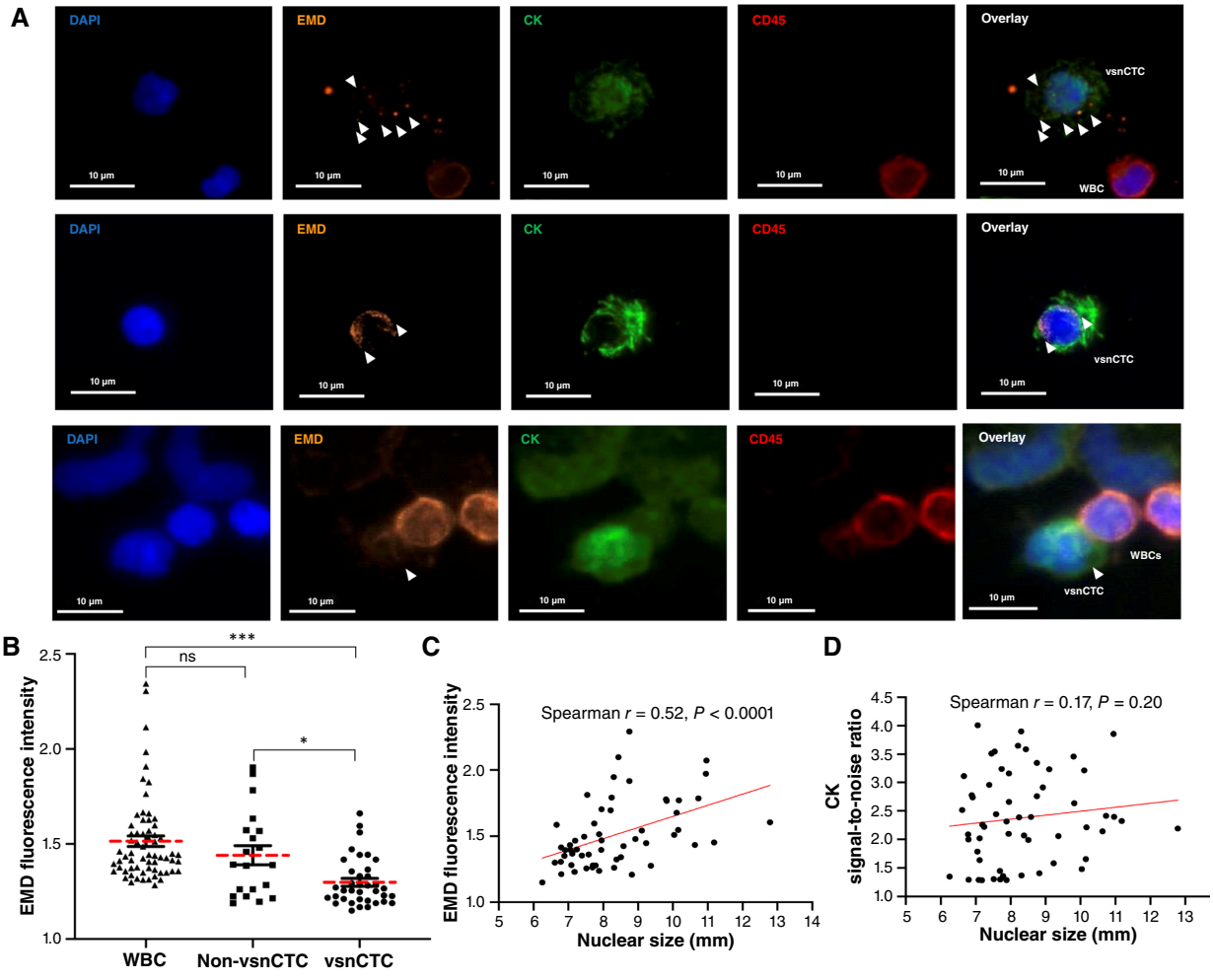

Figure 2.

Patients who are vsnCTC+ have CTCs with decreased EMD expression. **A,** EMD expression in vsnCTCs by a fluorescence microscope. DAPI (blue), EMD (orange), CK (green), and CD45 (red) staining is shown (scale bar, 10 μm). The vsnCTCs (<8.5 μm, DAPI+/CK+/CD45⁻) were stained with EMD. Arrows, EMD-positive punctate structures. **B,** EMD expression in individual WBCs, non-vsnCTCs, and vsnCTCs. **C,** Spearman correlation between EMD expression and the nucleus size of the CTC in patients with mCRPC. **D,** Spearman correlation between CK expression and the nucleus size of the CTC in patients with mCRPC. *, $P < 0.05$; ***, $P < 0.001$; ns, nonsignificant.

worse OS with increasing CTC numbers; however, the 95% CI frequently crossed an HR of 1.0, indicating limited statistical significance (Supplementary Fig. S3). Multivariable Cox regression adjusting for the minimum CTC nuclear size, PSA, baseline presence of VM, and CRPC treatments prior to the blood draw showed that the minimum CTC nuclear size was independently associated with OS (HR = 0.81, 95% CI, 0.70–0.95; $P = 0.0099$; Supplementary Table S4). This finding suggested that an increase of 1 μm in the minimum CTC nuclear size was linked to a 19% decrease in mortality risk.

CTCs from patients who are vsnCTC+ exhibit signs of nuclear shape instability by decreased EMD expression

To examine whether the vsn phenotype is a result of nuclear shape instability, we compared EMD expression from CTCs between patients with vsnCTC+ mCRPC and vsnCTC− mCRPC. Expression of EMD in white blood cells (WBC; CK^-, $CD45^+$, and $DAPI^+$) from patients with prostate cancer was utilized as a comparator. Immunofluorescence analysis showed that patients who were vsnCTC+ exhibited a loss of EMD along with mislocalization of EMD into puncta as described previously (**Fig. 2A**; ref. 20). Additionally, EMD expression was significantly decreased in CTCs from patients with vsnCTC+ mCRPC when compared with patients with vsnCTC− mCRPC (**Fig. 2B**, $P < 0.05$) and WBCs ($P < 0.0001$) at the single-cell level. There was no significant difference in EMD expression in CTCs from vsnCTC− patients and WBCs ($P = 0.32$). A significant positive correlation was observed between the EMD expression and the nuclear size of CTCs from patients with mCRPC (**Fig. 2C**, Spearman $r = 0.52$, $P < 0.0001$). In contrast, no significant correlation was found between CK and nuclear size (**Fig. 2D**, Spearman $r = 0.17$, $P = 0.20$), suggesting that the reduction in nuclear size was associated with the loss of EMD expression in CTCs from patients with advanced prostate cancer.

Depletion of EMD evokes the emergence of the vsn phenotype and promotes invasion and lineage plasticity *in vitro*

To examine the causal relationship between EMD loss and the vsn phenotype, we developed EMD-depleted cell lines by siRNA. DU145/EMD− cells exhibited nuclei that were 22% smaller than controls (**Fig. 3A** and **B**; $P < 0.001$). The EMD knockdown in 22Rv1 and C4-2B cells by siRNA similarly exhibited a 16% and 19% reduction in nuclear size respective to their isogenic control lines ($P < 0.0001$, $P < 0.0001$; **Fig. 3C** and **D**; Supplementary Fig. S4). The C4-2B/EMD− cells also had elevated invasiveness, as determined by transwell migration assay when compared with C4-2B/control (Ctrl) cells ($P < 0.01$; **Fig. 3E**).

As prostate cancers progress in the face of AR suppression, more poorly differentiated histologic phenotypes emerge that can exhibit small cell morphologic features or neuroendocrine features such as the expression of chromogranin A, synaptophysin, or other IHC markers of this phenotype (27). It is known that after multiple lines of antiandrogen therapies, 20% to 25% of mCRPCs will have a shift in gene expression consistent with the development of a neuroendocrine phenotype marked by expression of genes associated with cellular plasticity and stemness (28, 29). Given the increased invasiveness following EMD loss, along with the clinical associations of vsnCTCs with ARSI resistance, VM, and multiple lines of CRPC treatments, we next investigated whether EMD loss is associated

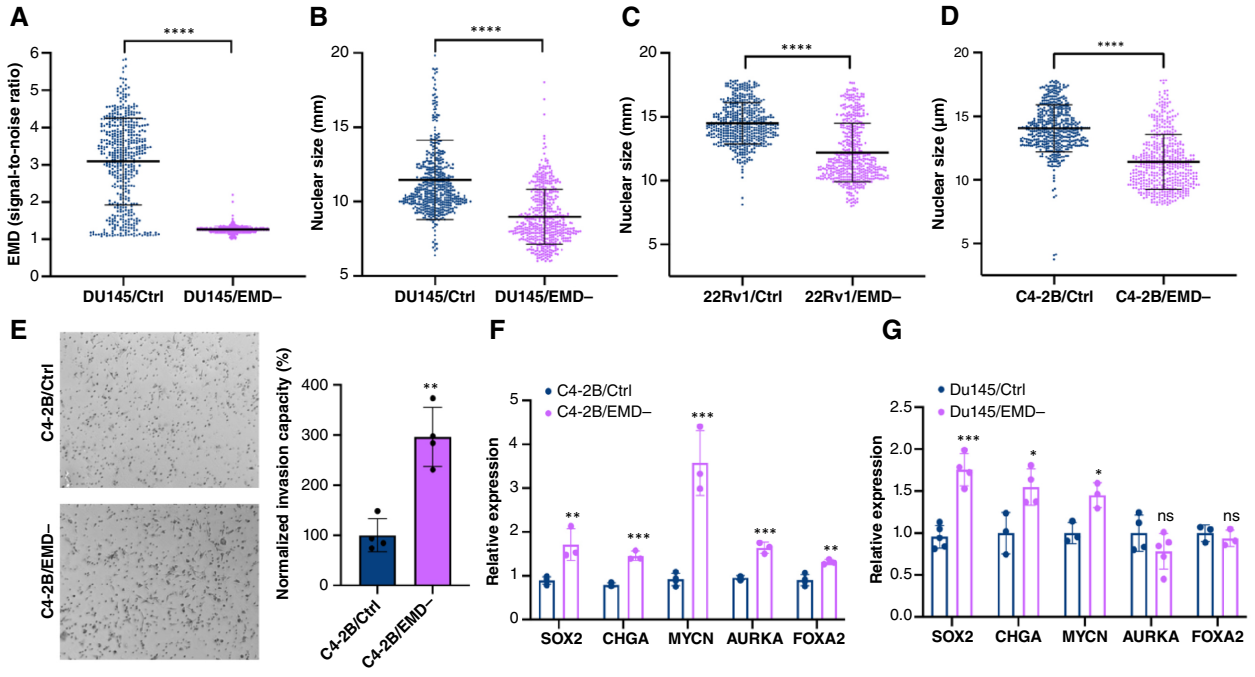

Figure 3.

Loss of EMD results in the vsn phenotype of decreased nuclear size, increased invasiveness, and features suggesting lineage plasticity. **A,** EMD expression by immunofluorescence in DU145 EMD knockdown cells by siRNA. **B–D,** Nuclear size of (**B**) DU145, (**C**) 22Rv1, and (**D**) C4-2B EMD knockdown cells by siRNA. **E,** EMD knockdown induces invasion in C4-2B EMD knockdown cells by siRNA. **F** and **G,** Expression of lineage plasticity markers in (**F**) C4-2B and (**G**) DU145 EMD knockdown cells by siRNA. *, $P < 0.05$; **, $P < 0.01$; ***, $P < 0.001$; ****, $P < 0.0001$; ns, nonsignificant.

with lineage plasticity. We identified markers associated with lineage plasticity based on published studies (30–32). In addition to increased invasiveness, C4-2B/EMD− cells showed elevated expression of genes associated with lineage plasticity (**Fig. 3F**), with similar findings observed in DU145/EMD− cells (**Fig. 3G**).

Transcriptomic changes in EMD knockdown cells

We next sought to uncover the molecular mechanisms underlying the role of EMD in prostate cancer biology. To do this, we performed GSEA on RNA-Seq data following EMD knockdown (Supplementary Fig. S5) to identify pathway enrichment in prostate cancer cells. Given that EMD knockdown is associated with the vsn phenotype and promotes lineage plasticity, metastasis, epithelial–mesenchymal transition, and dedifferentiation, these gene sets were found to be the most significantly upregulated pathways following the loss of EMD (**Fig. 4A–C**).

In addition, *KRAS* signaling, which is known to be associated with cancer stemness and metastatic progression in prostate cancer (33, 34), was enriched in EMD knockdown prostate cancer cells. Interestingly, we also observed an enrichment of *RB1*-loss–related pathways in EMD knockdown cells. As RB1 downregulation has been implicated in the transition from CRPC to a neuronally differentiated form (35, 36), this finding suggested that EMD loss could potentially contribute to this transition. These results are consistent with our data showing that EMD loss is associated with lineage plasticity.

ARSI-resistant cells exhibit a vsn phenotype and EMD loss

Given that patients who are vsnCTC+ demonstrate higher ARSI resistance compared with patients who are vsnCTC−, we next examined nuclear size in a well-established model of C4-2B ARSI-resistant cell lines developed by Liu and colleagues (23, 37). We observed that the C4-2B/Abi-R and C4-2B/Enza-R sublines exhibited a significant reduction in nuclear size (18.7% and 21.3%, respectively) compared with parental control cells (C4-2B/parent), as measured by the NanoVelcro assessment method (**Fig. 5A**), confirmed by confocal imaging (**Fig. 5B**). No statistically significant difference in nuclear size was observed between C4-2B/Abi-R and C4-2B/Enza-R cells. The EMD expression was found to be significantly reduced in both C4-2B/Abi-R and C4-2B/Enza-R cells compared with C4-2B/parent cells (**Fig. 5C**). In line with our observation that EMD loss is associated with the vsn phenotype, we found that the invasion capacity was higher in C4-2B/Abi-R and C4-2B/Enza-R cells compared with C4-2B/parent cells (**Fig. 5D**).

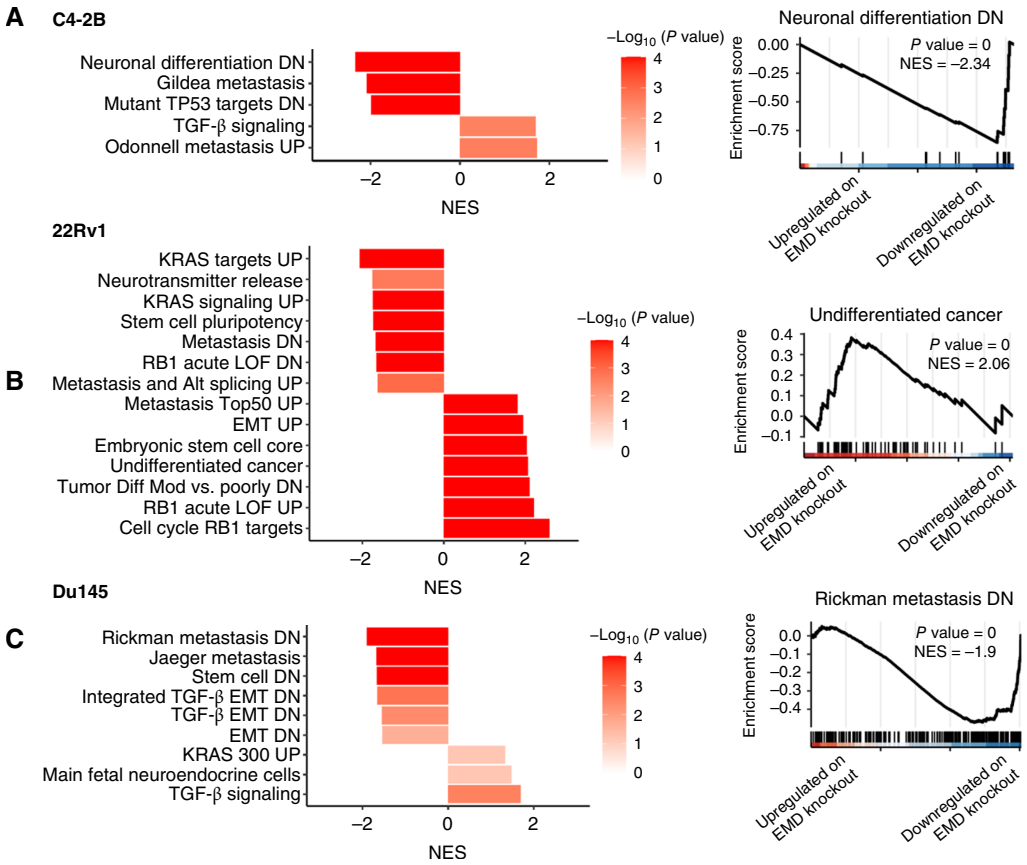

Figure 4.

EMD knockdown induces metastasis- and dedifferentiation-related pathways in prostate cancer cells. **A–C,** Bar graph depicting GSEA results for enriched pathways associated with metastasis and dedifferentiation. Representative GSEA enrichment plots are shown for EMD knockdown by shRNA in (**A**) C4-2B, (**B**) 22Rv1, and (**C**) DU145 cells, compared with nontargeting controls. EMT, epithelial–mesenchymal transition; NES, normalized enrichment score; UP, Up; DN, Down; Alt, alteration; LOF, loss of function; Diff, difference; Mod, Modulation.

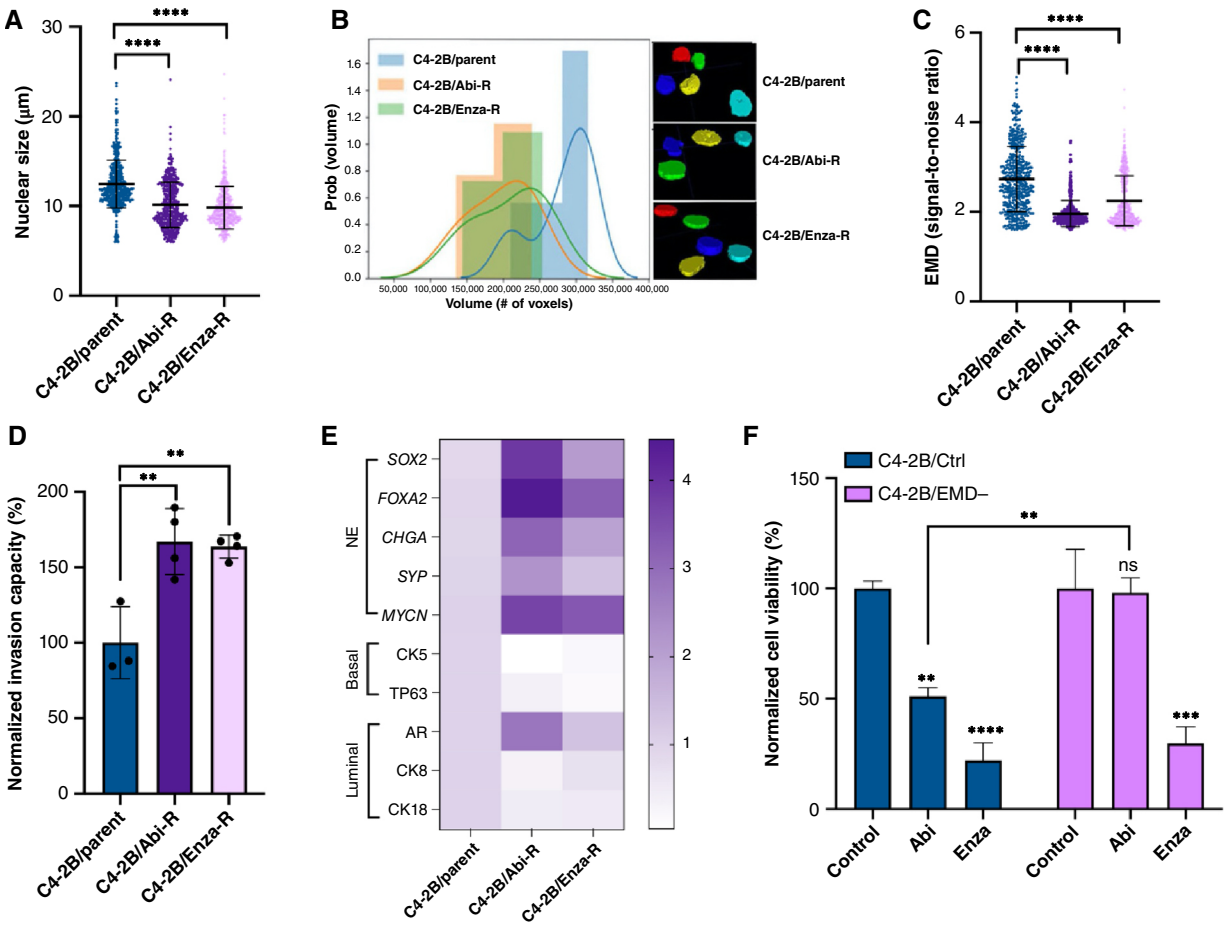

Figure 5.

Characterization of ARSI impact on vsn cells and morphologic and molecular features of ARSI-resistant cells. **A** and **B,** Nuclear size measurements of ARSI-resistant C4-2B sublines and parental controls by (**A**) NanoVelcro assay and (**B**) confocal microscopy. **C,** EMD expression in C4-2B ARSI-resistant sublines was assessed by immunofluorescence. **D,** Invasion capacity of C4-2B ARSI-resistant sublines by transwell assay. **E,** The expression of lineage plasticity markers in C4-2B ARSI-resistant sublines. NE, neuroendocrine. **F,** Cell viability of C4-2B EMD knockdown cells by siRNA after 5 days of treatment with 10 μmol/L Abi acetate and 1 μmol/L Enza. **, $P < 0.01$; ***, $P < 0.001$; ****, $P < 0.0001$.

These findings prompted us to explore whether lineage plasticity, a known pathway for therapeutic resistance, is present in ARSI-resistant C4-2B cell lines, based on previously established studies (30–32). Interestingly, our results indicated that neuroendocrine differentiation markers were upregulated in the C4-2B ARSI-resistant sublines, whereas basal markers were downregulated (**Fig. 5E**). These results are consistent with our findings that EMD loss is linked to lineage plasticity in prostate cancer cell lines.

To determine whether cells with EMD loss, which exhibit the vsn phenotype, have differential sensitivity to ARSI therapy, we compared the sensitivity of AR+ prostate cancer cells with EMD knockdown to their parental controls when treated with ARSIs. We selected C4-2B cells as they are castration-resistant cells but sensitive to ARSIs. Treatment of C4-2B/Ctrl cells with 10 μmol/L Abi acetate for 5 days significantly reduced cell viability (**Fig. 5F**, $P < 0.001$). In contrast, Abi had no effect on C4-2B/EMD− cells, indicating that C4-2B/EMD− cells were more resistant to Abi compared with the control cells (**Fig. 5F**). We also found 22Rv1/EMD− cells were relatively resistant to Abi when compared with control cells (Supplementary Fig. S6A). This resistance maybe due to EMD's close association with the endoplasmic reticulum (ER), in which Abi acts by inhibiting *CYP17* (38). As EMD is located on the nuclear envelope, which is continuous with the ER, its disruption could impair ER function, contributing to Abi resistance.

We also treated the C4-2B sublines with Enza. Surprisingly, despite the loss of EMD, these cells remained sensitive to Enza. Enza significantly inhibited the viability of C4-2B/EMD− cells (**Fig. 5F**, $P < 0.01$). When comparing impact of Enza on the C4-2B/EMD− and C4-2B/Ctrl cells, the viability of C4-2B/EMD− cells remained higher than that of C4-2B/Ctrl cells though the difference was not statistically significant. In addition, we found 22Rv1/EMD− cells exhibited a similar response to Enza as the control cells (Supplementary Fig. S6B). This finding suggested that the preserved sensitivity of the EMD knockdown in C4-2B and 22Rv1 cells to Enza may be due to nuclear instability caused by EMD loss, which would not affect the ability of Enza to block AR nuclear translocation (39), ultimately reducing cell viability.

Platinum-based chemotherapy demonstrates greater efficacy in castration-resistant tumor cells with the vsn phenotype

As the emergence of vsnCTCs and the vsn phenotype precedes the onset of VM, we hypothesized that the biological changes driving the vsn phenotype would increase the sensitivity of the underlying disease to platinum-based chemotherapy. To test this hypothesis, we compared the platinum sensitivity of vsn phenotype cells (DU145/EMD−) with non-vsn phenotype cells (DU145/Ctrl; **Fig. 6**). Our data demonstrated that DU145/EMD− cells exhibited a higher degree of cell death when exposed to cisplatin compared with DU145/Ctrl cells across various doses, suggesting the potential benefit of platinum-based chemotherapy in this context.

Discussion

Our previous work with vsnCTCs prompted studies to clarify the clinical significance of these observations and explore the biological mechanisms underlying these nuclear alterations. We found that the association of VM with vsnCTCs has evolved into a clear link with shortened OS and PFS. Our data suggested that vsnCTCs could serve as a visual indicator of increasing cellular plasticity, potentially guiding more tailored patient management strategies. These findings highlight the clinical relevance of vsnCTCs as indicators of aggressive disease.

EMD interacts with several proteins, including nuclear lamins and SUN-domain proteins, which play a crucial role in maintaining the structural integrity of the nuclear envelope (40). The loss of EMD leads to abnormal nuclear shapes and altered nuclear morphology, including the formation of blebs in the nuclear membrane (41). The nuclear envelope is essential for regulating the transport of molecules between the nucleus and the cytoplasm, influencing cell invasion and metastatic potential (42). Consequently, it was reasonable for the knock down of EMD to result in reduced nuclear size and concomitant changes in gene expression that promoted cellular aggressiveness and plasticity. Studies have shown that EMD deficiency enhances the invasive capacity of cells by reducing nuclear size and promoting an amoeboid phenotype (20, 43). Our previous research highlighted the connection between EMD dysregulation, nuclear shape instability, and metastatic potential in prostate cancer (20), prompting us to further investigate the relationship between EMD and the vsn phenotype.

Our analysis revealed that patients who were vsnCTC+, associated with EMD loss, had reduced PSA response rates following ARSI treatment and poor prognosis in patients with mCRPC. We found that the vsn phenotype could be reproduced by knocking down EMD in multiple prostate cancer cell lines, irrespective of AR expression status. We observed that downregulation of EMD had parallel increases in invasiveness and the expression of genes related to lineage plasticity. Notably, our findings indicated that ARSI-resistant cell lines had a smaller nuclear size compared with their isogenic parental cells. Consistently, we observed that these ARSI-resistant C4-2B cells exhibited lower EMD expression, further supporting the idea that EMD loss is linked to the vsn phenotype in prostate cancer. Additionally, these resistant cells displayed higher invasion capacity and greater lineage plasticity than their parental counterparts. This highlighted the pivotal role of EMD dysregulation in driving the vsn phenotype and its association with an aggressive subtype of mCRPC. Additionally, our data revealed that EMD knockdown of C4-2B cells exhibits increased resistance to Abi compared with control cells, while preserving sensitivity to Enza. This differential response may be attributed to the distinct mechanisms of these two drugs (38, 39). This finding may have clinical implications, particularly for treating patients with vsnCTCs, who may exhibit similar resistance patterns.

The onset of lineage plasticity raises clinical concerns about the need to change therapy. Following docetaxel, cabazitaxel has been shown to yield a survival benefit for patients with mCRPC (44). However, resistance to cabazitaxel eventually emerges in the patients with mCRPC that was refractory to treatment with ARSIs. The addition of platinum-based chemotherapy to either docetaxel or cabazitaxel in mCRPC has been shown to elicit a secondary response, which has become a therapy of interest in cases with anaplastic (45–47) or neuronal/neuroendocrine differentiation (44, 48). In fact, the use of platinum-based salvage chemotherapy for taxane-refractory, mCRPC has long been established (49). This observation of platinum sensitivity, however, contrasts with historical data indicating that mCRPC is generally not highly sensitive to platinum (50, 51). Notably, platinum-based chemotherapy is often introduced late in the clinical course (e.g., when VM are already visible on

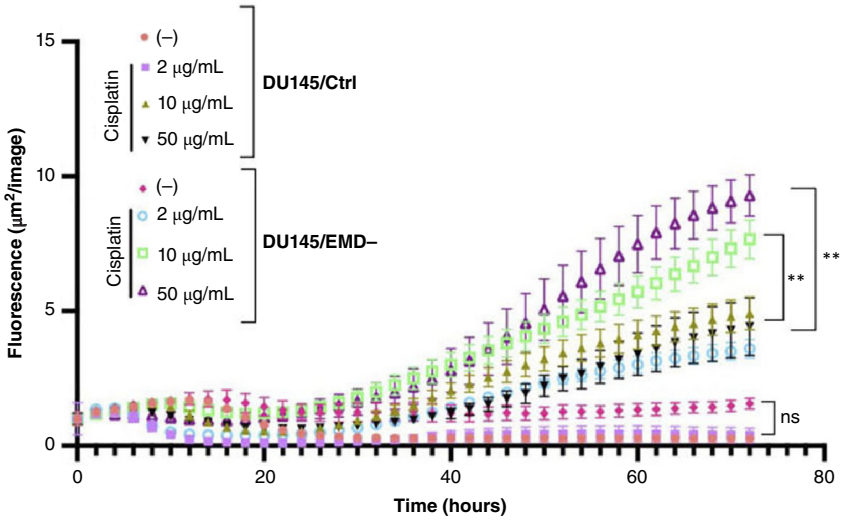

Figure 6.

Cisplatin sensitivity of vsn (DU145/EMD−) and non-vsn cells (DU145/Ctrl). Fluorescent quantification of cell death was measured using Incucyte Cytotoxicity Assay in real time. 1×10^4 DU145/EMD− and DU145/Ctrl cells were plated in 96 wells and incubated overnight. Cytotox Green (Incucyte Cytotoxicity reagent) was added simultaneously with cisplatin (at indicated concentrations). Results from triplicated wells are shown. **, $P < 0.001$; ns, nonsignificant.

conventional imaging), potentially reducing its benefits for the patients at that stage. Therefore, there is an opportunity to initiate this therapy earlier, when the disease burden is lower, and the cancer begins to exhibit sensitivity to platinum. Our findings revealed that vsn cells exhibit greater sensitivity to platinum-based chemotherapy compared with non-vsn cells, highlighting the potential of platinum-based chemotherapy as a valuable treatment option for vsnCTC+ mCRPC.

Our study has several unique and important features. First, the samples that were characterized were obtained from a single practice. This did provide an opportunity for us to conduct deep annotations in an effort to associate clinical and biomarker data. Additionally, this single practice original allowed us to consider the approach to treatment, and monitoring was uniform across patients as this is standardized in the clinical practice at the Cedars-Sinai Cancer Center for Uro-Oncology Research Excellence clinic. Thus, there were no substantial variations in clinical care that affected survival outcomes. As such, we could put forward that the appearance of the vsnCTC was an event that typically occurred later in the natural history of the disease and after multiple rounds of anticancer treatment.

Despite these advantages, our experimental approach has important limitations. First, the small sample limited the generalizability of our findings and reduced the statistical power of our analyses. Next, our ability to explore the impact of visceral metastatic site was constrained. This is important given the established significance of metastatic sites on prognosis (52). Considering these factors, our findings should primarily be considered hypothesis-generating and do require further validation in larger, more diverse cohorts.

In conclusion, our findings indicate that as patients with prostate cancer develop relapse through treatment, the biological mechanisms that promote resistance and cellular plasticity also drive alterations in the nuclear envelope, resulting in a reduction in nuclear size and the emergence of the vsn phenotype. Clinically, this phenotype is associated with more aggressive and unfavorable prostate cancer behavior, leading to shorter survival outcomes. Our study highlights that EMD deficiency plays a pivotal role in driving the vsn phenotype and lineage plasticity and can contribute as a marker for a clinically aggressive subtype of prostate cancer. Furthermore, nuclear size and EMD expression status may be useful for identifying patients who are more likely to benefit from platinum-based chemotherapy. Our findings justify further characterization of the vsnCTC phenotype and its implications in guiding prostate cancer therapy to provide greater personalization of care.

Authors' Disclosures

H.M. Sandler reports being a member of the board of directors of ASTRO. T. Daskivich reports personal fees from Medical Education Speakers Network, EDAP TMS, and RAND and other support from Lantheus outside the submitted work. H.-R. Tseng reports grants from the NCI during the conduct of the study as well as a patent for University of California, Los Angeles pending. No disclosures were reported by the other authors.

Authors' Contributions

L. Zhang: Formal analysis, validation, investigation, methodology, writing–original draft, writing–review and editing. **P.-C. Teng:** Formal analysis, validation, investigation, methodology, writing–review and editing. **K.A. Cavassani:** Formal analysis, methodology. **J. Wang:** Software, formal analysis, investigation, methodology. **C. Grasso:** Data curation, software. **J. Watson:** Software, formal analysis, methodology. **Z. Chen:** Data curation. **K.-H. Tu:** Data curation. **B. Salumbides:** Data curation. **K. Rohena-Rivera:** Data curation. **L. Gevorkian:** Data curation. **M. Kim:** Data curation, formal analysis, writing–review and editing. **S. You:** Conceptualization, resources, software, formal analysis, supervision, funding acquisition, methodology, writing–review and editing. **D. Di Vizio:** Supervision, validation, methodology, writing–review and editing. **H.M. Sandler:** Resources, investigation, writing–review and editing. **T. Daskivich:** Resources, investigation, writing–review and editing. **N.A. Bhowmick:** Conceptualization, resources, formal analysis, supervision, investigation, visualization, project administration, writing–review and editing. **M.R. Freeman:** Conceptualization, supervision, investigation, visualization, methodology, project administration, writing–review and editing. **H.-R. Tseng:** Conceptualization, resources, formal analysis, supervision, funding acquisition, investigation, visualization, methodology, project administration, writing–review and editing. **J.-F. Chen:** Conceptualization, formal analysis, supervision, investigation, visualization, methodology, writing–review and editing. **E.M. Posadas:** Conceptualization, resources, data curation, formal analysis, supervision, funding acquisition, investigation, visualization, methodology, writing–original draft, project administration, writing–review and editing.

Acknowledgments

This project was supported by the following funding sources: NIH/NCI P01CA23345201A1 (to L. Gevorkian, S. You, D. Di Vizio, E.M. Posadas, and N.A. Bhowmick), NIH/NCI 5P01CA098912 (to N.A. Bhowmick, M.R. Freeman, H.-R. Tseng, and E.M. Posadas), NIH/NCI 5U01CA198900-01 (to P.-C. Teng, K.A. Cavassani, J. Wang, K.-H. Tu, B. Salumbides, S. You, H.-R. Tseng, and E.M. Posadas), NIH/NCI 1R01CA218356-01 (to L. Zhang, P.-C. Teng, K.A. Cavassani, J. Wang, Z. Chen, K.-H. Tu, B. Salumbides, L. Gevorkian, S. You, H.-R. Tseng, and E.M. Posadas), Department of Defense W81XWH-18-1-0576 (to J. Wang), Department of Defense PCRP W81XWH-16-1-0638 (to P.-C. Teng and J.-F. Chen), and T32 5T32CA240172-05 (to J. Watson). We would like to express our sincere gratitude to all patients who participated in this study, as well as their families. We also acknowledge the support of the Cedars-Sinai Cancer Developmental Funds, the Biobank and Research Pathology Resource Core, and the Urologic Oncology Bioinformatics Group at the Cedars-Sinai Medical Center.

Note

Supplementary data for this article are available at Clinical Cancer Research Online (http://clincancerres.aacrjournals.org/).

Received November 4, 2024; revised January 23, 2025; accepted March 6, 2025; posted first March 10, 2025.

References

1. Deng Z, Wu S, Wang Y, Shi D. Circulating tumor cell isolation for cancer diagnosis and prognosis. EBioMedicine 2022;83:104237.
2. Zhan Q, Liu B, Situ X, Luo Y, Fu T, Wang Y, et al. New insights into the correlations between circulating tumor cells and target organ metastasis. Signal Transduct Target Ther 2023;8:465.
3. Pantel K, Hille C, Scher HI. Circulating tumor cells in prostate cancer: from discovery to clinical utility. Clin Chem 2019;65:87–99.
4. Cieślikowski WA, Antczak A, Nowicki M, Zabel M, Budna-Tukan J. Clinical relevance of circulating tumor cells in prostate cancer management. Biomedicines 2021;9:1179.
5. Chen JF, Ho H, Lichterman J, Lu YT, Zhang Y, Garcia MA, et al. Subclassification of prostate cancer circulating tumor cells by nuclear size reveals very small nuclear circulating tumor cells in patients with visceral metastases. Cancer 2015;121:3240–51.
6. Jan YJ, Chen JF, Zhu Y, Lu YT, Chen SH, Chung H, et al. NanoVelcro rare-cell assays for detection and characterization of circulating tumor cells. Adv Drug Deliv Rev 2018;125:78–93.
7. Chen JF, Zhu Y, Lu YT, Hodara E, Hou S, Agopian VG, et al. Clinical applications of NanoVelcro rare-cell assays for detection and characterization of circulating tumor cells. Theranostics 2016;6:1425–39.
8. Mosquera JM, Beltran H, Park K, MacDonald TY, Robinson BD, Tagawa ST, et al. Concurrent AURKA and MYCN gene amplifications are harbingers of lethal treatment-related neuroendocrine prostate cancer. Neoplasia 2013;15:1–10.

9. Mather RL, Andrews H, Pandha H, Jachetti E, Micallef J, Wang Y, et al. The Open University's first one-day symposium on treatment-emergent neuroendocrine prostate cancer. Future Oncol 2020;16:147–9.
10. Quintanal-Villalonga Á, Chan JM, Yu HA, Pe'er D, Sawyers CL, Sen T, et al. Lineage plasticity in cancer: a shared pathway of therapeutic resistance. Nat Rev Clin Oncol 2020;17:360–71.
11. Imamura J, Ganguly S, Muskara A, Liao RS, Nguyen JK, Weight C, et al. Lineage plasticity and treatment resistance in prostate cancer: the intersection of genetics, epigenetics, and evolution. Front Endocrinol (Lausanne) 2023;14: 1191311.
12. Epstein JI, Pizov G, Steinberg GD, Carter HB, Pitcock R, Armas OA, et al. Correlation of prostate cancer nuclear deoxyribonucleic acid, size, shape and Gleason grade with pathological stage at radical prostatectomy. J Urol 1992; 148:87–91.
13. Khan MA, Walsh PC, Miller MC, Bales WD, Epstein JI, Mangold LA, et al. Quantitative alterations in nuclear structure predict prostate carcinoma distant metastasis and death in men with biochemical recurrence after radical prostatectomy. Cancer 2003;98:2583–91.
14. Veltri RW, Christudass CS, Isharwal S. Nuclear morphometry, nucleomics and prostate cancer progression. Asian J Androl 2012;14:375–84.
15. Veltri RW, Isharwal S, Miller MC, Epstein JI, Partin AW. Nuclear roundness variance predicts prostate cancer progression, metastasis, and death: a prospective evaluation with up to 25 years of follow-up after radical prostatectomy. Prostate 2010;70:1333–9.
16. Veltri RW, Khan MA, Miller MC, Epstein JI, Mangold LA, Walsh PC, et al. Ability to predict metastasis based on pathology findings and alterations in nuclear structure of normal-appearing and cancer peripheral zone epithelium in the prostate. Clin Cancer Res 2004;10:3465–73.
17. Denais C, Lammerding J. Nuclear mechanics in cancer. Adv Exp Med Biol 2014;773:435–70.
18. Berk JM, Tifft KE, Wilson KL. The nuclear envelope LEM-domain protein emerin. Nucleus 2013;4:298–314.
19. Holaska JM, Wilson KL. An emerin "proteome": purification of distinct emerin-containing complexes from HeLa cells suggests molecular basis for diverse roles including gene regulation, mRNA splicing, signaling, mechanosensing, and nuclear architecture. Biochemistry 2007;46:8897–908.
20. Reis-Sobreiro M, Chen JF, Novitskaya T, You S, Morley S, Steadman K, et al. Emerin deregulation links nuclear shape instability to metastatic potential. Cancer Res 2018;78:6086–97.
21. Grigoryeva ES, Tashireva LA, Alifanov VV, Savelieva OE, Vtorushin SV, Zavyalova MV, et al. The novel association of early apoptotic circulating tumor cells with treatment outcomes in breast cancer patients. Int J Mol Sci 2022;23:9475.
22. Jansson S, Bendahl PO, Larsson AM, Aaltonen KE, Rydén L. Prognostic impact of circulating tumor cell apoptosis and clusters in serial blood samples from patients with metastatic breast cancer in a prospective observational cohort. BMC Cancer 2016;16:433.
23. Liu C, Lou W, Zhu Y, Yang JC, Nadiminty N, Gaikwad NW, et al. Intracrine androgens and AKR1C3 activation confer resistance to enzalutamide in prostate cancer. Cancer Res 2015;75:1413–22.
24. Scher HI, Morris MJ, Stadler WM, Higano C, Basch E, Fizazi K, et al. Trial design and objectives for castration-resistant prostate cancer: updated recommendations from the prostate cancer clinical trials working group 3. J Clin Oncol 2016;34:1402–18.
25. Eisenhauer EA, Therasse P, Bogaerts J, Schwartz LH, Sargent D, Ford R, et al. New response evaluation criteria in solid tumours: revised RECIST guideline (version 1.1). Eur J Cancer 2009;45:228–47.
26. Strasak AM, Lang S, Kneib T, Brant LJ, Klenk J, Hilbe W, et al. Use of penalized splines in extended Cox-type additive hazard regression to flexibly estimate the effect of time-varying serum uric acid on risk of cancer incidence: a prospective, population-based study in 78,850 men. Ann Epidemiol 2009;19:15–24.
27. Conteduca V, Oromendia C, Eng KW, Bareja R, Sigouros M, Molina A, et al. Clinical features of neuroendocrine prostate cancer. Eur J Cancer 2019;121:7–18.
28. Liu S, Alabi BR, Yin Q, Stoyanova T. Molecular mechanisms underlying the development of neuroendocrine prostate cancer. Semin Cancer Biol 2022;86:57–68.
29. Davies AH, Beltran H, Zoubeidi A. Cellular plasticity and the neuroendocrine phenotype in prostate cancer. Nat Rev Urol 2018;15:271–86.
30. Ku SY, Rosario S, Wang Y, Mu P, Seshadri M, Goodrich ZW, et al. Rb1 and Trp53 cooperate to suppress prostate cancer lineage plasticity, metastasis, and antiandrogen resistance. Science 2017;355:78–83.
31. Mu P, Zhang Z, Benelli M, Karthaus WR, Hoover E, Chen CC, et al. SOX2 promotes lineage plasticity and antiandrogen resistance in TP53- and RB1-deficient prostate cancer. Science 2017;355:84–8.
32. Wang Z, Townley SL, Zhang S, Liu M, Li M, Labaf M, et al. FOXA2 rewires AP-1 for transcriptional reprogramming and lineage plasticity in prostate cancer. Nat Commun 2024;15:4914.
33. Wang XS, Shankar S, Dhanasekaran SM, Ateeq B, Sasaki AT, Jing X, et al. Characterization of KRAS rearrangements in metastatic prostate cancer. Cancer Discov 2011;1:35–43.
34. Weng CC, Ding PY, Liu YH, Hawse JR, Subramaniam M, Wu CC, et al. Mutant Kras-induced upregulation of CD24 enhances prostate cancer stemness and bone metastasis. Oncogene 2019;38:2005–19.
35. Han W, Liu M, Han D, Li M, Toure AA, Wang Z, et al. RB1 loss in castration-resistant prostate cancer confers vulnerability to LSD1 inhibition. Oncogene 2022;41:852–64.
36. Venkadakrishnan VB, Yamada Y, Weng K, Idahor O, Beltran H. Significance of RB loss in unlocking phenotypic plasticity in advanced cancers. Mol Cancer Res 2023;21:497–510.
37. Liu C, Armstrong C, Zhu Y, Lou W, Gao AC. Niclosamide enhances Abi treatment via inhibition of androgen receptor variants in castration resistant prostate cancer. Oncotarget 2016;7:32210–20.
38. Attard G, Reid AH, A'Hern R, Parker C, Oommen NB, Folkerd E, et al. Selective inhibition of CYP17 with Abi acetate is highly active in the treatment of castration-resistant prostate cancer. J Clin Oncol 2009;27:3742–8.
39. Tran C, Ouk S, Clegg NJ, Chen Y, Watson PA, Arora V, et al. Development of a second-generation antiandrogen for treatment of advanced prostate cancer. Science 2009;324:787–90.
40. Koch AJ, Holaska JM. Emerin in health and disease. Semin Cell Dev Biol 2014; 29:95–106.
41. Rowat AC, Lammerding J, Ipsen JH. Mechanical properties of the cell nucleus and the effect of emerin deficiency. Biophys J 2006;91:4649–64.
42. Denais CM, Gilbert RM, Isermann P, McGregor AL, te Lindert M, Weigelin B, et al. Nuclear envelope rupture and repair during cancer cell migration. Science 2016;352:353–8.
43. Lavenus SB, Vosatka KW, Caruso AP, Ullo MF, Khan A, Logue JS. Emerin regulation of nuclear stiffness is required for fast amoeboid migration in confined environments. J Cell Sci 2022;135:jcs259493.
44. van der Zande K, Tutuhatunewa-Louhanepessy RD, Hamberg P, Ras S, de Feijter JM, Dezentjé VO, et al. Combined cabazitaxel and carboplatin treatment of metastatic castration resistant prostate cancer patients, with innate or acquired resistance to cabazitaxel monotherapy. Clin Genitourin Cancer 2024; 22:445–53.e1.
45. Corn PG, Heath EI, Zurita A, Ramesh N, Xiao L, Sei E, et al. Cabazitaxel plus carboplatin for the treatment of men with metastatic castration-resistant prostate cancers: a randomised, open-label, phase 1-2 trial. Lancet Oncol 2019; 20:1432–43.
46. Ganeshan D, Aparicio AM, Morani A, Kundra V. Pattern and distribution of distant metastases in anaplastic prostate carcinoma: a single-institute experience with 101 patients. AJR Am J Roentgenol 2017;209:327–32.
47. Aparicio AM, Harzstark AL, Corn PG, Wen S, Araujo JC, Tu SM, et al. Platinum-based chemotherapy for variant castrate-resistant prostate cancer. Clin Cancer Res 2013;19:3621–30.
48. Akkus E, Arslan Ç, Ürün Y. Advancements in platinum chemotherapy for metastatic castration-resistant prostate cancer: insights and perspectives. Cancer Treat Rev 2024;130:102818.
49. Ross RW, Beer TM, Jacobus S, Bubley GJ, Taplin ME, Ryan CW, et al. A phase 2 study of carboplatin plus docetaxel in men with metastatic hormone-refractory prostate cancer who are refractory to docetaxel. Cancer 2008;112: 521–6.
50. Osborne CK, Blumenstein BA, Crawford ED, Weiss GR, Bukowski RM, Larrimer NR. Phase II study of platinum and mitoxantrone in metastatic prostate cancer: a Southwest Oncology Group Study. Eur J Cancer 1992;28: 477–8.
51. Huan SD, Stewart DJ, Aitken SE, Segal R, Yau JC. Combination of epirubicin and cisplatin in hormone-refractory metastatic prostate cancer. Am J Clin Oncol 1999;22:471–4.
52. Halabi S, Kelly WK, Ma H, Zhou H, Solomon NC, Fizazi K, et al. Meta-analysis evaluating the impact of site of metastasis on overall survival in men with castration-resistant prostate cancer. J Clin Oncol 2016;34:1652–9.